International Journal of Pharmaceutics 622 (2022) 121872

Contents lists available at ScienceDirect

International Journal of Pharmaceutics

journal homepage: www.elsevier.com/locate/ijpharm

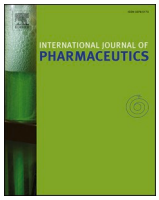

3D printing of customized all-starch tablets with combined release kinetics

Kizkitza González, Izaskun Larraza, Garazi Berra, Arantxa Eceiza, Nagore Gabilondo *

Department of Chemical and Environmental Engineering, 'Materials+Technologies' Group. Engineering College of Gipuzkoa, University of the Basque Country (UPV/EHU), Plaza Europa 1, 20018, Donostia-San Sebastián, Spain

ARTICLE INFO

Keywords:
3D printing
Starch
Ibuprofen
Oral tablets
Customized drug delivery

ABSTRACT

Starch-based tablets with tailored releases were prepared by 3D printing using a hydrophobic drug. The importance of the origin of the excipient in the inks and tablets was analyzed. Besides, the effect of the geometry of the tablet on the drug release profile was also evaluated. The rheological properties of the inks was influenced by the botanic origin of the starch. Consequently, tablets presented different microporous structure and particular compression and swelling behaviors. Normal maize starch showed a non-well-defined porous morphology, not being able to form a stable structure whereas, waxy maize and potato starches exhibited a well-defined porous structure and were both able to maintain their integrity after long time immersion. Finally, tablets combining different starches and geometries were printed tailoring the drug release from 10 min to 6 h and designing two-steps profiles. The applicability of the developed 3D printed drug release systems in personalized therapies was demonstrated.

1. Introduction

Traditional pharmaceutical processing methods produce drugs in batches with certain specifications and specific parameters (shape, size and type of release), but in much cases without meeting individual needs of patients such as genetic, age, gender or constitution, as well as severity and stage of the disease (Raijada et al., 2021; Zhu et al., 2020). Indeed, conventional pills are commonly based on adults' dosage, thus pediatric and elderly patients require age-appropriate doses (Raijada et al., 2021; Zhu et al., 2020). In addition, the mentioned patient subgroups also need specific dosage form alternatives to facilitate oral administration of drugs, such as flash delivery systems (Raju et al., 2011). In this sense, fast disintegrating tablets raise as a good option since they are immediately dissolved when placed in tongue and are rapidly released with saliva facilitating the swallowing (Parkash et al., 2011).

Another challenge that pharmaceutical companies should overcome is the development of new strategies to achieve the time-controlled release of hydrophobic drugs without compromising the safety and efficacy (Hsu et al., 2015; Kalepu and Nekkanti, 2015). Nowadays, the 40% of the marketed drugs and the 60% of the drug candidates in research are poorly water soluble leading to formulation problems in the design of novel intravenous or oral drug delivery systems (Fuhrmann et al., 2012; Hsu et al., 2015; Larrañeta et al., 2018). Thus, pharmaceutical researchers required new therapeutic compounds with controlled release profiles, avoiding heterogeneity and drug loading quantity limitations (Larrañeta et al., 2018).

In this context, the 3D printing technology is gaining attention as an advanced technique for personalized medicine and the development of on demand drug release tablets (O'reilly et al., 2021; Pandey et al., 2020). The 3D printing manufacturing process is a computer-aided design method (CAD) in which the material is deposited layer-by-layer to form a 3D object (Pandey et al., 2020; Zhu et al., 2020). This approach allows the production of custom-designed products, like different shaped tablets loaded with several drugs in different amounts, as well as adjustable release properties, which could not be produced using traditional methods (Goyanes et al., 2015; Olmos-Juste et al., 2021). The surface area and the volume of the 3D objects could tailored controlling its geometry, thereby customized drug release profiles could be achieved (Vithani et al., 2019). Furthermore, 3D printing is a versatile and easy-to-use manufacture technique with short production times and reduced material wastage (O'reilly et al., 2021).

In addition, some patients usually need several pills for the medical treatment of different diseases or to extend the therapeutic action of a single drug (Beg et al., 2020). Unlike conventional dosage forms, 3D printing allows the preparation of tailored polypills loaded with multiple doses of a drug or doses of multiple drugs (Robles-Martinez et al., 2019; Seoane-Viaño et al., 2021b). Indeed, by using 3D printing techniques the development of products ranging from fast disintegrating to extended-release tablets with great flexibility to optimize the dose,

* Corresponding author.

https://doi.org/10.1016/j.ijpharm.2022.121872
Received 8 March 2022; Received in revised form 23 May 2022; Accepted 24 May 2022
Available online 27 May 2022

shape and size of the dosage forms to meet the personal requirements is possible (Beg et al., 2020; Fina et al., 2017). Thus, on demand and custom-designed tablets can be produced in small batches to answer the individual therapeutic needs and physical conditions of each patient with lower production costs (Beg et al., 2020; Hongjian Li et al., 2020; Seoane-Viaño et al., 2020; Zhu et al., 2020).

Binder jetting, material extrusion, material jetting, direct powder extrusion (DPE) and semi-solid extrusion (SSE), selective laser sintering (SLS) and vat photopolymerization are the most commonly applied 3D printing technologies in pharmaceutical industry (Seoane-Viaño et al., 2021a). In this work SSE, also known as direct ink writing (DIW), was used. SSE is a material extrusion technique based on the deposition of semi-solid or semi-molten materials (gel or pastes) employing a syringe-like extrusion system (Seoane-Viaño et al., 2020; Seoane-Viaño et al., 2021a, Seoane-Viaño et al., 2021b). SSE allows the preparation of complex geometries with finer structures and shapes at low printing temperatures without the requirement of exclusive equipment (Bansal et al., 2018; Seoane-Viaño et al., 2021a, Seoane-Viaño et al., 2021b). The rheological properties of DIW inks must be investigated in detail since they require an appropriate shear thinning behavior to ensure the extrusion through the nozzle and enough yield stress and recovery capacity to avoid the collapse of the printed pieces (Ji et al., 2020).

Starch is widely used in the pharmaceutical industry as excipient for the preparation of drug delivery solid forms since it is digestible, nontoxic, nonirritant, multifunctional and versatile (Ashogbon and Akintayo, 2014; Builders and Arhewoh, 2016). Besides, from an industrial point of view it presents the economic advantage of its low cost, as it is one of the most abundant biopolymer and it could be obtained from a wide variety of plant sources, mainly tubers and cereals (Domene-López et al., 2019; González et al., 2018). As it is well known, two are the main macromolecular components of starch: amylose and amylopectin (González et al., 2015). Amylopectin is a highly branched D-glucose polysaccharide that facilitates the formation of gel-like starch materials though numerous intra- and inter-molecular H-bonding interactions, while in amylose the D-glucose arranges in a linear manner and is reassociated to form a non-soluble network structure (González et al., 2015; Onofre et al., 2009). In addition, starch contains traces of lipids (phospholipids and fatty acids) and phosphate monoesters (Pérez and Bertoft, 2010). The amylose/amylopectin ratio as well as other features such as granule morphology, the presence of other chemical compounds, gelatinization temperature, structural characteristics, molecular weight or crystallinity are dependent on the botanical origin of the starch (Domene-López et al., 2019; Kaur and Gill, 2003; Khan et al., 2017; Ogunsona et al., 2018; Onofre et al., 2009). Indeed, the effect of compositional differences of starches on their performance as matrices for sustained release has been comprehensively evaluated elsewhere (Elgaied-Lamouchi et al., 2021; Odeku, 2013; Onofre et al., 2009; Szepes et al., 2008). Moreover, several authors attributed specific gel properties to the higher phosphorous compounds of potato starch in comparison that from cereals (Domene-López et al., 2019), thus leading to specific starch gels behavior (Karim et al., 2007; Pérez and Bertoft, 2010).

However, as far as we know, there is no reported literature exploiting these differences for the design and fabrication of tailor-made tablets by combining starches from different resources. Traditionally, polymer blends have been proposed to adjust the desired drug delivery kinetics in a single tablet (Elgaied-Lamouchi et al., 2021; Lu et al., 2008) what sometimes could led to compatibility or printability concerns. On the contrary, starches from different botanical origin would offer distinguished release profiles, avoiding the incompatibility drawbacks, as it is, in essence, the same biopolymer.

The main aim of this work was to produce 3D printed starch-based tablets for tailored administration of hydrophobic drugs. Thus, we hypothesized that the use of starches from different botanical origin would lead to different drug release kinetics. In addition, we considered the geometry and the aspect ratio as other key factors to obtain a wide range of drug delivery profiles. Thus, firstly the gelatinization parameters of the three starches and the printability of their inks were analyzed. The influence of the botanical origin on the morphology, mechanical properties and swelling capacity of the 3D printed tablets was also evaluated. Finally, the feasibility of the 3D printing technique to prepare on demand starch-based tablets with tailored release profiles of ibuprofen as hydrophobic drug was thoroughly studied by drug delivery measurements.

2. Experimental

2.1. Materials

Normal maize (NM), waxy maize (WM) and potato (P) starches were purchased from Sigma-Aldrich (USA). Ibuprofen (IB, ≥98%) was acquired from Sigma-Aldrich. For the swelling and drug delivery tests, phosphate buffered saline (PBS) tablets were provided by Panreac (Spain). All reagents were employed as received. Distilled water was used as solvent.

2.2. Preparation of the starch-based inks

The inks were prepared by the gelatinization of three starches from different sources, i.e. normal maize, waxy maize and potato starches. Briefly, each starch was dispersed in distilled H_2O (30 wt%) and heated above the gelatinization temperature under continuous magnetic stirring for 20 min. The gelatinization of normal maize and waxy maize starches was performed at 90 °C, whereas 80 °C was used for potato starch. These unloaded inks have been named as NM30, WM30 and P30 for the normal maize, waxy maize and potato starches, respectively. For the preparation of the drug loaded inks, 5 mg of IB g^{-1} starch gel was added to the cooled gelatinized starch. In those cases, the inks have been named as L-NM30, L-WM30 and L-P30.

2.3. 3D printing procedure

The obtained starch gels were printed by using a Voladora 3D printer (Tumaker, S.L. Spain) adapted for layer-by-layer syringe extrusion (Fig. 1). All samples were printed with a needle of 0.8 mm in diameter, using 6 mm s^{-1} printing speed and 100% infill percentage. Tablets of two geometries were printed: cylinders of 10 mm in diameter and 5 mm in height (314.2 mm^2 in surface area and 392.7 mm^3 in volume, 0.80 aspect ratio) and pyramids of 12 mm in length, 12 mm in width and 7.2 mm in height (316.8 mm^2 in surface area and 345.6 mm^3 in volume, 0.92 aspect ratio). The printed samples were finally freeze-dried. Printed tablets were designated as $NM30_{3D}$, $WM30_{3D}$, $P30_{3D}$ (unloaded tablets) and L-$NM30_{3D}$, L-$WM30_{3D}$, L-$P30_{3D}$ (loaded tablets). In addition, loaded tablets were prepared combining normal maize starch and waxy maize starch (named as L-$NM30_{3D}$ + L-$WM30_{3D}$) as well as normal maize starch and potato starch, (named as L-$NM30_{3D}$ + L-$P30_{3D}$).

2.4. Characterization methods

Differential scanning calorimetry (DSC) was performed in a Mettler Toledo DSC3+ equipment. Samples with a weight between 5 and 10 mg were sealed in medium pressure pans (n = 3) and were heated from room temperature to 150 °C at 10 °C min^{-1} heating rate under nitrogen atmosphere. The gelatinization temperature (T_G) and enthalpy (ΔH_G) were calculated as the maximum and the area under the endothermic transition, respectively.

Thermogravimetric analysis (TGA) was performed using a Mettler Toledo TGA/DSC3+ instrument. The measurements were conducted from 25 to 800 °C, with a heating rate of 10 °C min^{-1} under nitrogen atmosphere.

X-ray diffraction measurements were performed in order to determine the crystallinity degree (CD) of the starches. All measurements were performed using a Philips Xpert Pro diffractometer operating at 40

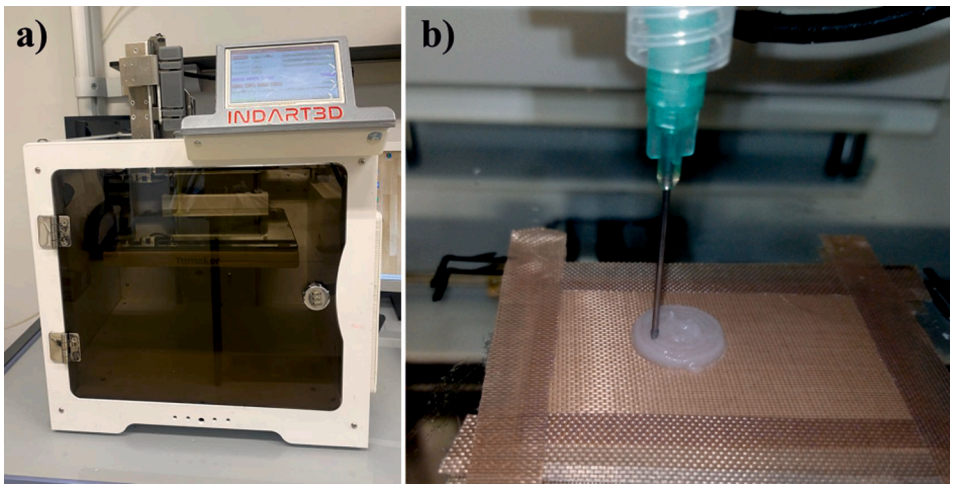

Fig. 1. a) Photography of Voladora 3D printer (Tumaker) and b) photography taken during the printing process.

kV and 40 mA, in θ - θ configuration secondary monochromator with Cu-Kα radiation (λ = 1.5418 Å) and a PIXcel solid state detector (active length in 2θ = 3.347°). Scattered radiation was detected in the angular range 1−40° (2θ). The crystallinity degree (CD) was calculated by the ratio of the crystallinity area to the total area (Dome et al., 2020):

$$CD(\%) = \frac{A_{Crystallinity}}{A_{Total}} \times 100 \quad (1)$$

where $A_{Crystallinity}$ is the area corresponding to the crystalline phase; and A_{Total} is the total area under the XRD pattern.

The appearance, size and morphology of the starch granules were evaluated by optical microscopy (OM) in transmission mode with a Nicon Eclipse E600 instrument.

Scanning electron microscopy (SEM) cross section images were recorded using a Hitachi S-4800N Field Emission Gun Scanning Electron Microscope (FEG-SEM) with an operation voltage of 5 kV. Samples were freeze-dried after swollen in distilled water and gold coated prior to the measurements.

The rheological characterization of inks was performed using a Haake Viscotester IQ rheometer (Thermo Fisher Scientific) equipped with a Peltier temperature controller system and a solvent trap. Gelatinization temperature was determined by temperature sweeps heating the initial starch/H_2O mixture (30 wt%) from 30 to 100 °C at a heating rate of 3 K min^{-1} using cone-plate geometry. Flow tests, oscillatory stress sweep test and recovery measurements were conducted for gelatinized starches (30 wt%) using parallel plate geometry (25 mm of diameter) at 20 °C. Flow test measurements were executed varying the shear rate between 0.2 and 500 s^{-1}, while the oscillatory shear stress sweep tests were performed between 1 and 10000 Pa. Yield point is determined as the stress at which storage modulus deviates from the linearity (Cyriac et al., 2015). The recovery tests were carried out measuring the storage modulus in a strain constant oscillatory test of three consecutive stages: 1) at 1% during 120 s; 2) at 50% during 300 s; and 3) at 1% during 120 s. The rheological measurements were all conducted in triplicate, n = 3.

Compression tests (n = 5) of printed tablets were performed using an Universal Testing Machine Instron 5967 with a load cell of 50 N at room temperature. Cylindrical samples of 10 mm in diameter and 5 mm in height were tested at 5 mm min^{-1} crosshead rate.

The swelling capacity of tablets (n = 3) was determined by traditional gravimetric method. Freeze-dried hydrogels were incubated at 37 °C until equilibrium in PBS at pH = 7.4. At selected time intervals, the swollen hydrogels were taken out, the water excess was removed with a filter paper and the sample weighed. The Swelling Ratio (SR) was determined by the Eq. (2):

$$SR(\%) = \frac{W_s - W_t}{W_t} \times 100 \quad (2)$$

where W_s is the weight of the swollen sample and W_t is the weight of the final dried sample. The equilibrium swelling was considered to be achieved when the weight of the samples no longer increased.

For drug delivery measurements Ibuprofen (IB) was selected as the model hydrophobic drug for *in vitro* release studies in a simulated intestinal medium (PBS). For the release studies, the freeze-dried drug loaded tablets were stirred in 100 mL of PBS solution (pH = 7.4) at 37 °C. At selected time intervals, an aliquot of 1 mL of the solution was taken out and analyzed by UV–vis spectroscopy. After that, the aliquot was returned to the beaker. The amount of released IB was determined by comparing the absorbance signal at 221.5 nm (maximum absorbance wavelength of IB) with a standard calibration curve. The Cumulative Release (CR) at each time interval was calculated using the Eq. (3):

$$CR(\%) = \frac{m_t}{m_0} \times 100 \quad (3)$$

where m_t is the cumulative mass of IB released at time t and m_0 is the total loaded amount of IB.

3. Results and discussion

3.1. Study of the gelatinization

The gelatinization of the three starches (NM, WM and P) was evaluated by calorimetry conducting dynamic heating measurements of the initial 30 wt% starch/water mixture. As defined elsewhere the gelatinization of the starch granules is an endothermic first order transition (H. Liu et al., 2009; Taghizadeh and Favis, 2013).

The obtained DSC thermograms and the determined ΔH_G and T_G results are displayed in Fig. 2a and Table 1, respectively. As it could be observed, the gelatinization was clearly detected in the three cases and denoted as G. Both the ΔH_G and T_G values were found to be dependent on the botanical origin of the starch. As it was reported previously (Abdullah et al., 2018), the thermal behavior would be affected by the characteristics of granules, such as crystallinity degree, chemical composition or morphology. The crystallinity of the three starches was determined by X-ray diffraction as the ratio of the crystallinity area to the total area (Figure S1). Comparing the two maize starches, NM, with 27% amylose, presented a relative crystallinity degree of 33.8%, while WM, containing only trace amounts of amylose, showed a relative crystallinity of 39.0%. The higher amylopectin content as well as the higher crystallinity degree resulted in higher ΔH_G and T_G values for the

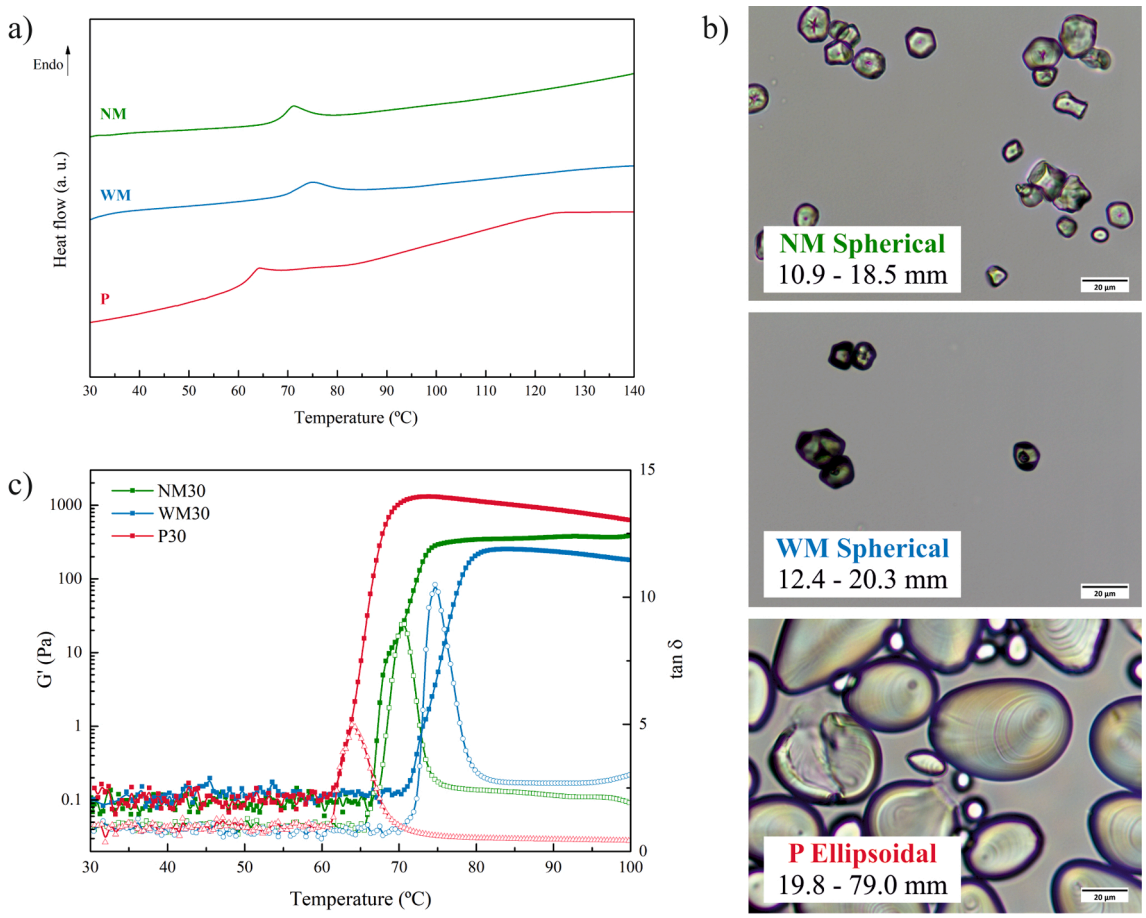

Fig. 2. a) DSC measurements of initial starch/water mixtures, b) morphology of starch granules (scale bar, 20 μm) and c) rheological measurements.

Table 1
Gelatinization temperatures obtained by DSC and rheological measurements.

Sample	ΔH_G (J g^{-1}) *DSC*	T_G (°C) *DSC*	G'_{max} (Pa)	tan δ	T_G (°C) *Rheology*
NM	2.8 ± 0.1	70.4 ± 0.6	471 ± 16	1.7 ± 0.0	70.3
WM	3.2 ± 0.4	73.3 ± 1.1	229 ± 20	2.7 ± 0.0	74.6
P	4.4 ± 0.2	64.7 ± 0.4	1426 ± 189	0.7 ± 0.0	64.0

latter. In contrast, potato starch containing 25% of amylose (Larrea-Wachtendorff et al., 2019) exhibited a relative crystallinity degree value of 34.6%, similar to that of NM. However, it is worthy to note that significantly higher content of phosphorous compounds has been usually attributed to potato starch, what it seemed to be responsible of the detected highest ΔH_G and lowest T_G values. In order to corroborate this statement, the ash content of the three starches was measured by TGA (Figure S2) since, as defined elsewhere (Schirmer et al., 2013), it would be representative of the phosphorous compounds content of the starch. The results were 11.8%, 12.6% and 15.5% for NM, WM and P, subsequently, corroborating reported literature and thus supporting the transition temperature and enthalpy variations observed by DSC.

As mentioned, the granule morphology would also be a critical issue when comparing different behavior of starches. For that reason, the size and morphology of granules were studied by optical microscopy. As observed in Fig. 2b, granules of both normal and waxy maize starches were ranged between 10 and 20 μm and presented quite spherical shape. In contrast, potato starch granules were ellipsoidal and presented a wide size dispersion, ranging from 20 to 80 μm. The larger and more irregularly shaped granules of potato starch could also be affecting the aforementioned highest ΔH_G as well as the lowest T_G values and broader transition range (Schirmer et al., 2013).

On the other hand, the gelatinization of normal maize, waxy maize and potato starches was also evaluated by oscillatory rheological measurements performing temperature sweeps (Fig. 2c and Table 1).

As compared in Table 1, the T_G values obtained by rheological measurements were in concordance with those results obtained by DSC. Indeed, the lowest gelatinization temperature for potato starch was corroborated (64.0 °C) followed by normal maize starch (70.3 °C) and waxy maize starch (74.6 °C). Considering the above-mentioned results and, in order to ensure that the crystalline domains of the native starch granules will be destroyed, 90 °C was chosen to carry out the gelatinization of normal maize and waxy maize starches, whereas 80 °C was used for potato starch.

As observed, all samples presented quite similar rheological pattern involving three main steps. During the first step at lower temperatures G' presented almost constant and low values. The second step started right before the gelatinization temperature was reached. At this time, G' increased dramatically and a maximum of tan δ was observed. In the last step, above the gelatinization temperature a maximum value of the storage modulus was achieved, G'_{max}.

As shown in Table 1, NM and WM presented lower G'_{max} values compared with that for P since ellipsoidal and larger potato starch granules remaining in the gel could led to higher G'_{max} and lower tan δ values (Kaur and Gill, 2003). Further increase of the temperature provoked the decrease of the G'_{max} value, as a result of the rupture of remaining starch granules, the breakage of the intermolecular hydrogen bonding and the reduction of chain entanglements (Chen et al., 2019). Besides, the high phosphate monoester content as well as the absence of lipids and phospholipids in potato starch favored the increase of G'_{max} leading to a more elastic gel.

3.2. Characterization of unloaded inks and printed tablets

3.2.1. Rheological characterization of unloaded inks

The rheological characterization is essential to predict the ulterior behavior of the inks during the 3D printing process. All the results obtained from the rheological measurements of unloaded inks are collected in Fig. 3 and Table S1.

The printability of the three starchy inks was assessed by conducting flow tests (Fig. 3a), where the decrease of the viscosity as the shear rate increased was appreciated in the studied range. This rheological behavior could be described by power-law (Chen et al., 2019), defined by the following Equation:

$$\eta = K\dot{\gamma}^{n-1} \quad (4)$$

where Î· is the viscosity, $\dot{\gamma}$ is the shear rate, K is the consistency coefficient and n is the power-law index. The results were adjusted to the Eq. (4) and the obtained values are collected in Table S1.

In all cases the power-law index was $n < 1$, thus indicating non-Newtonian fluid character and presenting the required shear-thinning behavior (Huijun Li et al., 2016). However, results showed that the shear thinning behavior of the inks was dependent on the starch source. Indeed, NM30 ink showed the lowest n value, indicating larger dependence of the viscosity on the shear rate and marked shear thinning behavior (Z. Liu et al., 2019). Besides, P30 sample exhibited the highest K value and hence the highest viscosity value, often attributed to the specific morphology of potato starch granules and its greater swelling capacity (Cisneros et al., 2009; Singh et al., 2002).

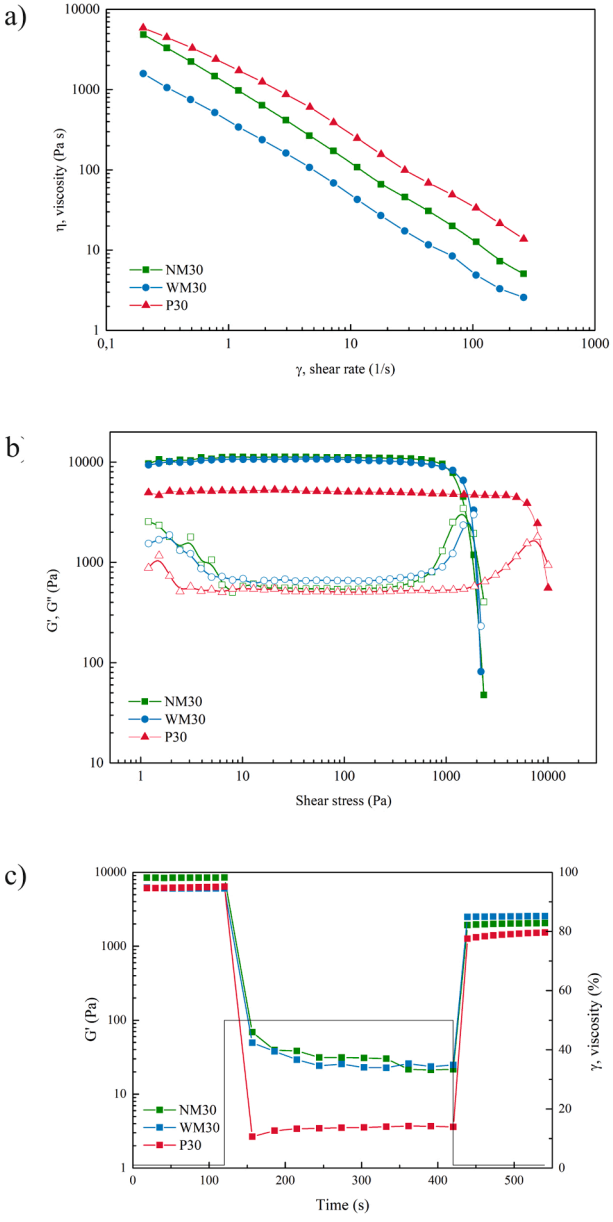

Fig. 3. Rheological measurements of unloaded inks.

Printability and shape fidelity were analyzed by means of stress sweep measurements (Fig. 3b). Results showed that in all cases G' was almost constant and higher than G'' revealing solid gel-like behavior. In addition, it should be noticed that both NM30 and WM30 inks presented higher G' values compared with P30.

On the other hand, yield stress (τ_y) and flow stress (τ_f) were determined as the shear stress value where G' loses the linearity and the crossover between G' and G'' (not shown), subsequently (Cyriac et al., 2015; Vadillo et al., 2021). As showed in Table S1, the two maize starch based NM30 and WM30 inks presented similar τ_y and τ_f values, whereas considerably higher values were measured for P30. The lowest lipid content of potato starch may favor the starch/starch interactions resulting into a stronger network with higher τ_y and τ_f values. Chen et al. (2019) reported similar stress values for potato and maize starch slurries at 20% (w/w), even if higher G' values at low stress were detected in that case for potato starch. It should be noted that the solid content of the slurry and the gelatinization temperature would notably affect to the rheological values of the inks. According to our flow tests results, it could be affirmed that potato-based inks would result harder to be extruded through the nozzle whereas waxy or normal maize could lead to stronger 3D printed tablets.

Finally, recovery tests were also carried out to simulate the printing process and analyze the thixotropic behavior of the inks. The monitored response of the inks over time is depicted in Fig. 3c.

As explained in the Experimental Section, the recovery test involves three steps. In the first step, the state of the ink before printing was simulated. Later, in order to reproduce the printing process conditions, the strain was increased resulting in the decrease of G' due to the structure breakdown. Finally, the strain was decreased and G' suddenly grew up again. As observed, it could be concluded that all samples showed the needed thixotropic response. Thus, recovery values of around 20% were obtained for NM30 and P30, while WM30 presented a recovery capacity of 41.5%. These relatively low recovery values could be indicating that the initial physical entanglements were not completely recovered.

As observed by rheological results, P30 presented the highest viscosity values. Although some authors (Yang et al., 2018b) argued that higher viscosities could led to an improved shape fidelity, in our case the potato starch-based ink showed worst accuracy. Indeed, potato starch ink was visually sticky and during the printing process, the material adhered to the nozzle blocking it. These processability difficulties led to a quite harder printability and accuracy defects. In contrast, normal maize starch and waxy maize starch-based inks were smoothly printed and less defects were observed. In concordance with (Zheng et al., 2019), it could be corroborated that higher viscosities and faster gelatinization of starch could difficult the printing process.

3.2.2. 3D printing and characterization of unloaded starch-based tablets

Cylindrical and pyramidal tablets were successfully 3D printed with normal maize, waxy maize and potato starch inks. The cross-section morphology of the freeze-dried tablets was evaluated by SEM (Fig. 4). As it is well known, interconnected porous internal architecture is desirable for drug delivery applications, since the porous network would facilitate the transport and delivery of the desired drug molecules outside the swollen polymeric network (González et al., 2018; Lima-Tenório et al., 2015).

Waxy maize and potato starch-based tablets presented interconnected porous microstructure although they showed remarkably

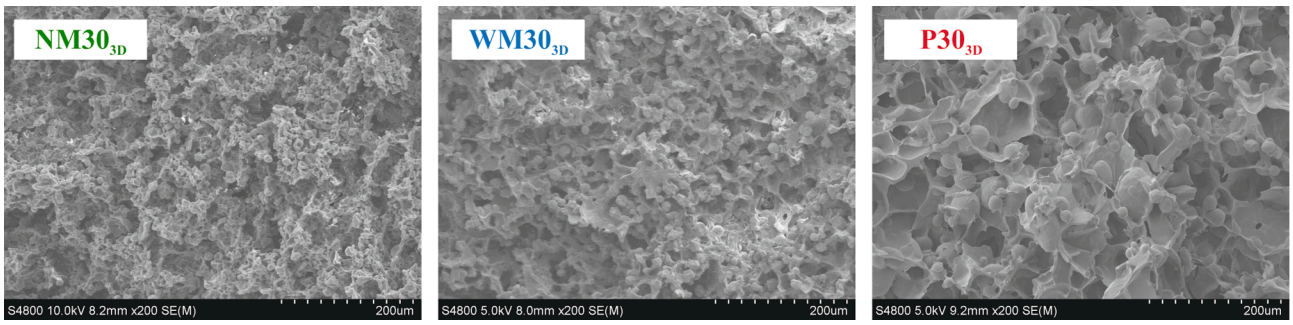

Fig. 4. SEM images of the microstructure of unloaded tablets.

differences regarding pore size and wall thickness. In the case of normal maize starch-based sample, quite compact morphology was obtained, and a well-defined homogeneous pore structure was not observed. Potato starch tablets presented higher pore size (around 100 μm), while 20 μm was measured for waxy maize starch samples.

In addition, the prepared cylindrical tablets were characterized in terms of compression behavior since the mechanical behavior is one of the most important key quality factors of pharmaceutical tablets (Mazel et al., 2016). The obtained compressive properties are shown in Table 2.

The stress vs strain curves of all samples presented the typical compression pattern involving three regions: i) an initial elastic zone, ii) followed by a plateau and ii) an ending densification slope (Mane et al., 2017; Salimi Jazi et al., 2014). Although the same compression pattern was shown for all samples, the mechanical behavior of the designed tablets was strongly influenced by the botanical origin.

As it could be observed, $NM30_{3D}$ sample showed higher Young's modulus and stress at yield point values compared to both $WM30_{3D}$ and $P30_{3D}$ tablets, increasing up to 20.7 MPa and 1.2 MPa, respectively. During this initial step, the cell walls started to bend and the absence of a porous microstructure in the $NM30_{3D}$ sample did not allow the cell walls to bend, behaving as a continuous solid and giving rise to higher Young's modulus and stress at yield point.

When increasing the load, the stress plateau related to the plastic behavior was reached (Salimi Jazi et al., 2014). During this step, the cell walls started to buckle and yield, until collapsing. The further increase of the strain led to the crush and densification of the collapsed cells, resulting in the rapid increase of the stress (Mane et al., 2017). As noticed, $P30_{3D}$ tablet showed higher densification strain attributable to the homogenous porous microstructure with remarkably larger pore size observed by SEM, leading the cell walls to collapse and come in contact at higher strain values (Ugarte et al., 2015).

The swelling capacity is another crucial factor of the tablets since it would be associated with the release mechanism of the loaded drug out of the swollen network (González et al., 2020). Thus, the swelling ratio (SR) was measured in order to evaluate the feasibility of the developed tablets to be used as drug release systems. The measurements were carried out gravimetrically by swelling freeze-dried samples (n = 3) in PBS at 37 °C and pH = 7.4 (Fig. 5).

Both waxy maize and potato starch-based tablets swelled and maintained their integrity after long time immersion in PBS. On the contrary, the swelling measurement of $NM30_{3D}$ tablets was not possible since they immediately disintegrated after immersion in PBS. In the case of waxy maize starch, this behavior could be associated to the high branched amylopectin content that resulted in strong amylopectin-amylopectin intermolecular interactions (Onofre et al., 2009) leading to a robust matrix capable to retain fluids. In the case of potato starch, even if it contains much lower amylopectin to amylose ratio, the higher molecular weight of both polysaccharides as well as the larger phosphorous content (Kaur and Gill, 2003; Onofre and Wang, 2009) led to strong network structure capable of the swelling while keeping the integrity. Normal maize starch, with lower amylopectin to amylose ratio and less phosphorous substances, did not form enough interactions to obtain stable swelled network.

Regarding the swelling profile, a first step where the SR increased rapidly in a short period followed by a second one where the SR value remained in equilibrium almost constant (220%) was observed in both $WM30_{3D}$ and $P30_{3D}$ tablets. However, it should be pointed out that the equilibrium swelling ratio was achieved faster for $P30_{3D}$. The differences on the internal porous microstructure seemed to be decisive to shorten the first swelling period for potato starch-based tablets. Indeed, the higher pore size of $P30_{3D}$ facilitates the faster permeation of PBS through the starch polymeric network.

These results suggested that waxy maize and potato starch samples would present continuous and quite longtime drug release, whereas normal maize tablets could be good candidate for burst release of flash administration applications. These remarkable differences regarding the integrity and swelling capacity of the tablets provided the opportunity to design polypills by the combination of different starches for the loading and tailored release of hydrophobic drugs.

Table 2
Mechanical properties of NM30, WM30 and P30.

Sample	Young's module (MPa)	Stress (at Yield Point) (MPa)	Densification strain (%)
NM30	20.7 ± 1.4	1.6 ± 0.2	44.2 ± 2.6
WM30	10.0 ± 0.6	0.8 ± 0.4	47.4 ± 1.5
P30	10.3 ± 0.6	0.4 ± 0.1	57.6 ± 0.5

3.3. Characterization of loaded inks and printed tablets

3.3.1. Rheological characterization of loaded inks

The rheological behavior of the Ibuprofen (IB) loaded inks was also evaluated (Fig. 6 and Table S2). Concerning flow test results (Fig. 6a), a significant increase of *n* was noticed in all cases comparing with the unloaded inks, indicating less pronounced shear thinning behavior, particularly for the L-P30 ink. Besides, it could be observed that the viscosity of the inks decreased, especially at low shear rates. As reported in literature, IB, as well as other drugs, could exhibit some plasticizing capacity due to the formation of polymer/drug interactions that disturbs the H-bonds between polymer chains, thus decreasing the viscosity of the gel (Soares et al., 2013; Wiranidchapong et al., 2015; Censi et al., 2018).

Fig. 6b presents the stress sweep measurements of loaded inks. Results showed the decrease of G', τ_y and τ_f, especially for the potato starch-based ink. These results corroborated the hypothesis of plasticizing effect of IB and the occurrence of strong polymer/drug interactions. It seemed that IB formed stronger interactions with potato starch leading to a higher plasticization degree and the reduction of G' value. Furthermore, when the drug behaves as plasticizer the free volume between polymer chains increase (Van Renterghem et al., 2017), thus improving the processability which is reflected in a decrease of both τ_y and τ_f.

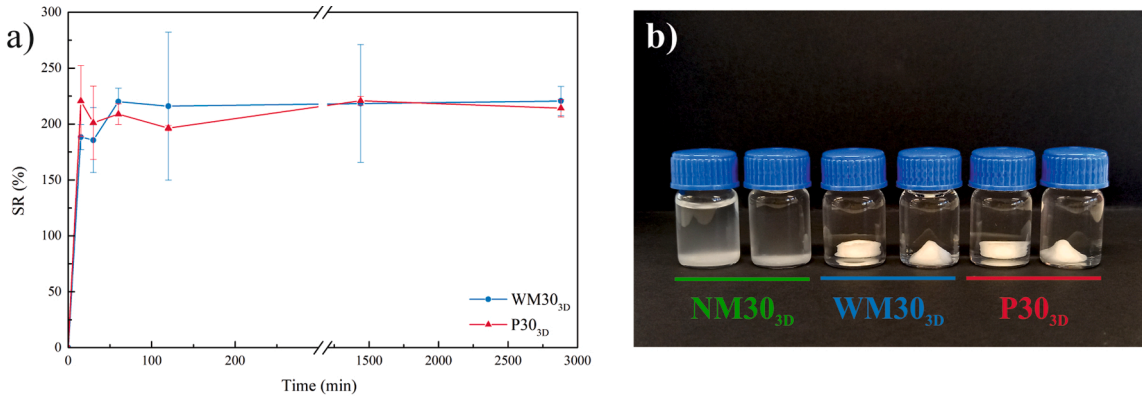

Fig. 5. a) SR (%) versus time curves and b) images after 1 h of swelling of NM30$_{3D}$, WM30$_{3D}$ and P30$_{3D}$ tablets in PBS at 37 °C.

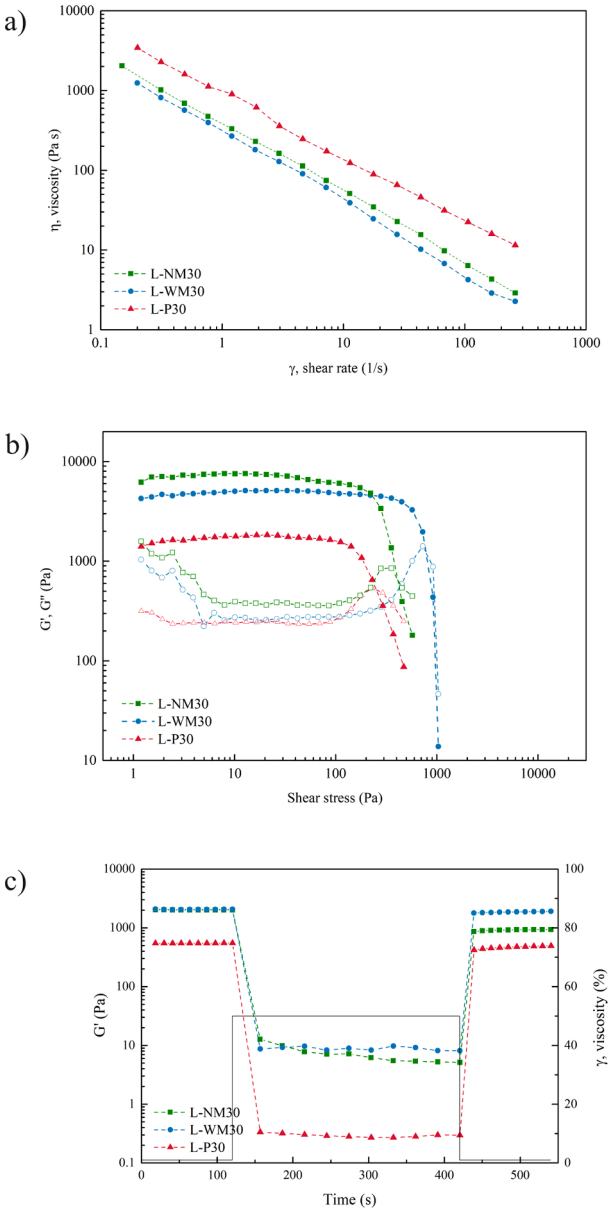

Fig. 6. Rheological measurements of loaded inks.

Finally, recovery test of loaded inks (Fig. 6c) showed that the recovery capacity was enhanced after the incorporation of IB. The results would be indicating that the new IB/starch physical interactions entanglements were recovered easier in comparison with the starch/starch H bonding interactions. Both L-WM30 and L-P30 inks achieved recovery values higher than 75%, almost doubling that of the unloaded starch inks and, hence, predicting their feasibility to be printed through the syringe needle as well as its capability to support the next printing layer without deformation (Chen et al., 2019; Z. Liu et al., 2018).

3.3.2. 3D printing of starch-based loaded tablets

In the case of loaded inks, cylindrical and pyramidal loaded tablets were also successfully printed with normal maize, waxy maize and potato starch inks. Additionally, loaded tablets composed of normal and waxy maize starch inks or normal maize and potato starch inks in combination were also printed. The CAD designs and images of the resulting loaded tablets are shown in Fig. 7.

All the loaded inks were adequately 3D printed, maintained the programmed CAD geometries and presented good cohesion capacity, which is in concordance with the suitability for 3D printing predicted by rheological results. However, regarding the accuracy of the dimensions of the pieces, those obtained with normal maize and waxy maize starches presented better shape fidelity than those of potato starch, which plays an important role in quality of the product in 3D printing technology (Yang et al., 2018a; Zheng et al., 2019). As demonstrated by flow tests, loaded normal and waxy maize starch-based inks exhibited lower n values, leading to an improved shear thinning behavior for L-NM30$_{3D}$ and L-WM30$_{3D}$ inks whereas a worse printability was observed for L-P30$_{3D}$ ink. Furthermore, potato starch-based ink showed a lower G' value resulting in inappropriate layer deposition, thus corroborating a better shape fidelity for L-NM30$_{3D}$ and L-WM30$_{3D}$ samples.

In addition, as concluded for unloaded inks, the printing process of the potato starch-based ink was laborious due to its high viscosity and sticky behavior. These difficulties obstruct the nozzle during the printing process and resulted in a poor accuracy of the tablets prepared using L-P30. In contrast, normal maize starch and waxy maize starch presented hardly defects and a better accuracy compared with their 3D CAD models.

3.3.3. Characterization of the 3D printed tablets

Waxy maize, normal maize and potato starch loaded tablets were individually assessed as sustained drug delivery systems. Additionally, in view of the different swelling behavior and the flash release ability of normal maize starch, the combination of normal maize starch with waxy maize or potato starches in a single loaded tablet was also tested. In addition, cylinder and pyramid shaped tablets were printed in order to study the influence of the geometry in the drug release kinetics.

The morphology of the freeze-dried IB loaded tablets was also analyzed by SEM in order to evaluate the influence of the addition of IB

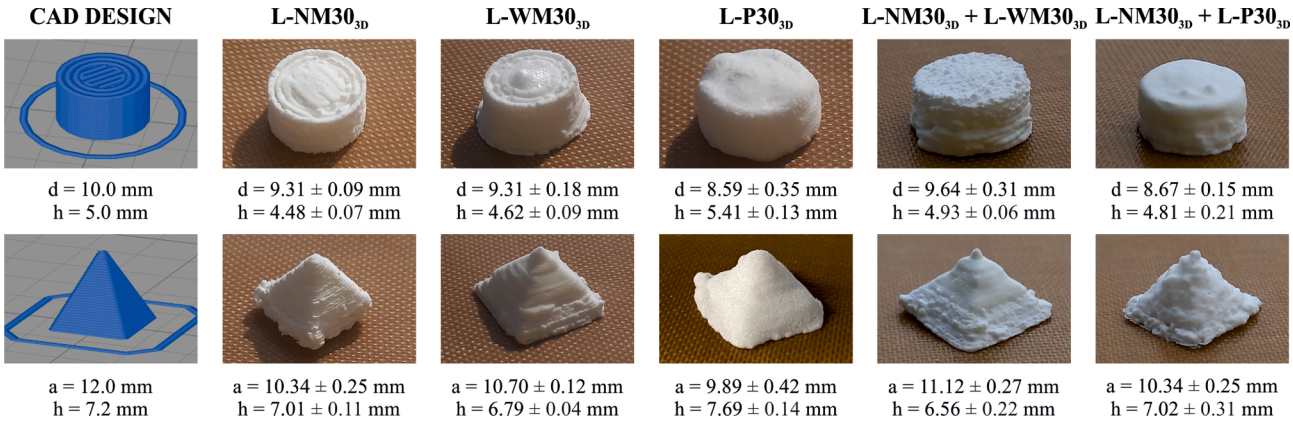

Fig. 7. CAD design and starch-based 3D printed loaded tablets with different geometrical shapes.

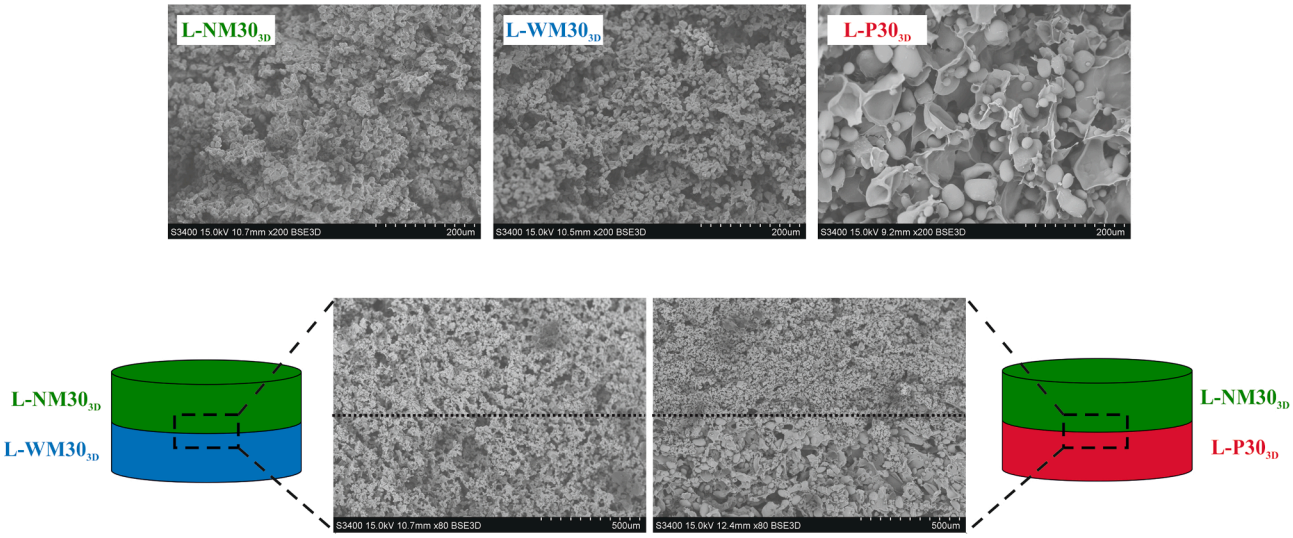

Fig. 8. SEM images of the microstructure of loaded a) L-NM30$_{3D}$, L-WM30$_{3D}$ and L-P30$_{3D}$ and b) L-NM30$_{3D}$ + L-WM30$_{3D}$ and L-NM30$_{3D}$ + L-P30$_{3D}$ tablets.

in the internal porous structure of the samples. As presented in Fig. 8a, no remarkable differences were observed regarding the morphology of both unloaded and loaded tablets indicating that the morphology was not influenced by the addition of IB. In addition, the Fig. 8b shows the morphology of the tablets prepared combining two starch types. The images were captured in the middle of the tablet in order to observe the interphase between both starches. In agreement with previous conclusions and as seen in Fig. 4, the morphology differences of each part were clearly appreciable.

In order to analyze the physical state of the drug in the final formulations, DSC and X-ray diffraction measurements were performed. DSC thermograms are shown in Figure S3. The DSC curve of ibuprofen presented an endothermic peak located around 75 °C related to the melting of the drug. On the other hand, in the case of unloaded tablets, no thermal transition was observed in the evaluated temperature range. In contrast, all loaded tablets showed a peak near 75 °C associated to the melting of IB.

In addition, the crystallinity of IB on loaded tablets was also analyzed (Figure S4). As it could be observed, raw normal maize and waxy maize starches presented peaks located at 2θ = 15.2°, 2θ = 17.3°/18.2° and 2θ = 23.3° related to the A-type polymorphism of starch (González et al., 2020). On the other hand, native potato starch is classified as B-type polymorphism which exhibited several peaks centered at 2θ = 5.8°, 2θ = 15.1°, a strong peak at 2θ = 17.2°, 2θ = 22.4° and 2θ = 24.1° (Cheng et al., 2022). In contrast, after gelatinization and 3D printing procedures, all unloaded tablets presented a low intensity residual peaks located around 2θ = 20°, indicating that the crystalline regions were almost destroyed (Cheng et al., 2022; Dash et al., 2013). In the case of loaded tablets, all samples presented new peaks associated with the presence of crystalline IB located at 2θ = 6.2°, 2θ = 16.7°, 2θ = 17.6°, 2θ = 20.2° and 2θ = 22.3°. These results are in concordance with DSC analysis, concluding that the crystalline nature of the IB remained intact after the 3D printing process.

The drug delivery evaluation of freeze-dried tablets was carried out using IB as hydrophobic model drug at 37 °C during 24 h in PBS. At established time intervals, an aliquot from the release medium was taken and measured by UV–vis spectroscopy.

The obtained drug release profiles are shown in Fig. 9.

On the one hand, as it could be observed in Fig. 9a, L-NM30$_{3D}$ showed immediate release of the drug once it was immersed and disintegrated in the release medium wherein, in 10 min the loaded IB was almost completely detected (close to 95%). These results demonstrated the viability of normal maize starch-based tablets to be used in applications where burst or flash release is required. For instance, L-NM30$_{3D}$ could be employed as orally disintegrating tablets, particularly for those patients who present swallowing difficulties since it could be completely disintegrated in mouth cavity with saliva (Badgujar and Mundada, 2011; Comoglu and Unal, 2015).

On the other hand, both L-WM30$_{3D}$ and L-P30$_{3D}$ tablets showed a sustained release profiles where the IB cumulative release reached 90%

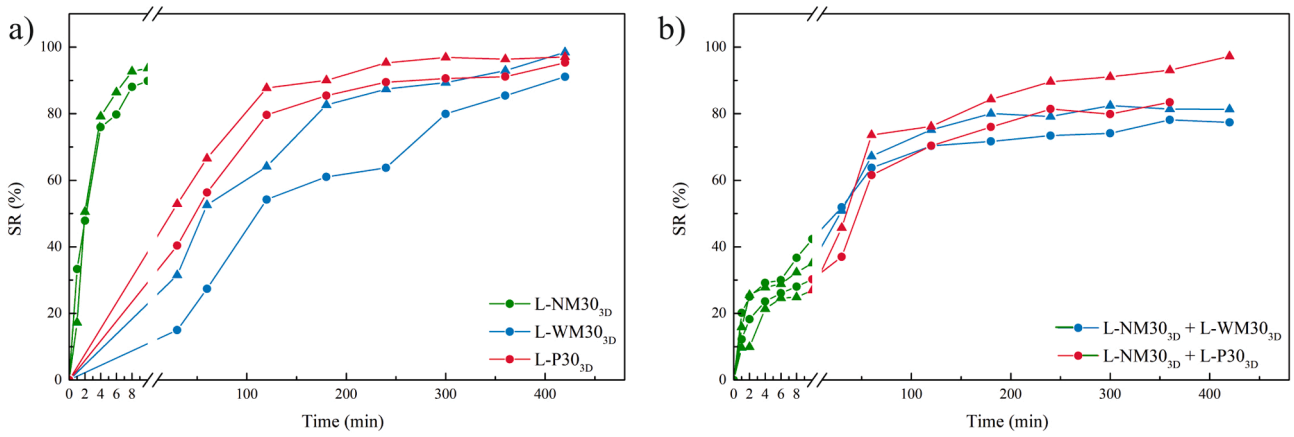

Fig. 9. Drug release profiles in PBS at 37 °C of a) L-NM30$_{3D}$, L-WM30$_{3D}$ and L-P30$_{3D}$ tablets and b) L-NM30$_{3D}$ + L-WM30$_{3D}$ and L-NM30$_{3D}$ + L-P30$_{3D}$ tablets. Cylindrical tablets were indicated as (●) and pyramidal tablets as (▲).

after 7 h. In the case of L-WM30$_{3D}$, a longer lasting sustained release was observed whereas the IB was faster released for L-P30$_{3D}$. These results were in agreement with the observed swelling patterns and suggested that the release of IB would be directly related to the ability of the release medium to penetrate and swell the tablet.

The drug release profiles obtained with the combination of different starches in the tablets are shown in Fig. 9b. As it can be observed, the combination of the two starches allowed the initial fast release of the drug loaded in the normal maize starch part, i.e. half of the total amount of IB loaded, while releasing the rest of the drug in a sustained manner. Indeed, mainly in the case of the combination of the two maize starches, the 40% of the loaded IB was released to the medium in the first 10 min, whereas near 50 min were required for the neat waxy maize tablet for the same release amount. It should also be mentioned that the partial disintegration of the tablet seemed to accelerate the release from the potato or waxy maize parts, mainly in the case of the latter. However, the occurrence of disintegrated maize starch increased the viscosity of the release medium and, hence, influenced the total released amount from the piece.

Regarding the influence of the geometry on the release kinetics of IB, it could be noticed that the pyramidal shaped tablets facilitated the release whereas cylindrical pills presented more sustained profile. The higher surface area to volume ratio of pyramidal forms led to faster drug delivery (Goyanes et al., 2015), demonstrating the relevance of the size and geometry of the tablets on the release pattern.

4. Conclusions

Starch-based pharmaceutical tablets were successfully obtained by 3D printing manufacturing, following a quick an easy methodology that allowed the preparation of tablets with different geometries loaded with a non-soluble drug. Firstly, the gelatinization process of starches was analyzed by DSC and rheological measurements. As expected, the gelatinization temperature was affected by the botanical origin of the starch. Secondly, it was demonstrated that all inks presented the required rheological behavior for adequate printability. In addition, as considered, the mechanical behavior, as well as the swelling capacity and, in consequence, the drug release properties were found to be dependent of the microstructure, porosity degree, the chemical composition (amylopectin/amylose ratio and the presence of other components) of the starch and the ability to the formation of an effective network structure. It was corroborated that the drug release could be tailored optimizing the suitable starch type and tablet shape. Thus, the obtained starch-based 3D printed tablets showed promising properties in view of future personal drug release applications.

CRediT authorship contribution statement

Kizkitza González: Methodology, Investigation, Writing – original draft. **Izaskun Larraza:** Methodology, Investigation, Visualization. **Garazi Berra:** Methodology, Investigation. **Arantxa Eceiza:** Conceptualization, Supervision. **Nagore Gabilondo:** Conceptualization, Writing – review & editing, Supervision.

Declaration of Competing Interest

The authors declare that they have no known competing financial interests or personal relationships that could have appeared to influence the work reported in this paper.

Acknowledgments

Financial support from the University of the Basque Country (UPV/EHU) (GIU18/216 Research Group), from the Basque Government in the frame of Elkartek KK-2020/00053 and PIBA2020-1-0041 and from Spanish Ministry of Science and Innovation and Spanish State Research Agency (MCIN/AEI/10.13039/501100011033) in the frame of PID2019-105090RB-I00 project, are gratefully acknowledged. Moreover, we are grateful to the Macrobehavior-Mesostructure-Nanotechnology SGIker unit of the UPV/EHU. K. González thanks the University of the Basque Country for the grant "Contratación de doctores recientes hasta su integración en programas de formación postdoctoral en la UPV/EHU «DOKBERRI» 2020-I" (DOCREC20/07).

Data Availability

The data will be made available on request.

Appendix A. Supplementary data

Supplementary data to this article can be found online at https://doi.org/10.1016/j.ijpharm.2022.121872.

References

Abdullah, A.H.D., Chalimah, S., Primadona, I., Hanantyo, M.H.G., 2018. Physical and chemical properties of corn, cassava, and potato starchs. IOP Conf. Ser.: Earth Environ. Sci. 160 (1) https://doi.org/10.1088/1755-1315/160/1/012003.

Ashogbon, A.O., Akintayo, E.T., 2014. Recent trend in the physical and chemical modification of starches from different botanical sources: A review. Starch/Staerke 66 (1–2), 41–57. https://doi.org/10.1002/star.201300106.

Badgujar, B.P., Mundada, A.S., 2011. The technologies used for developing orally disintegrating tablets: A review. Acta Pharmaceutica 61 (2), 117–139. https://doi.org/10.2478/v10007-011-0020-8.

Bansal, M., Sharma, V., Singh, G., Harikumar, S.L., 2018. 3D printing for the future of pharmaceuticals dosages forms. Int. J. Appl. Pharm. 10 (3), 1–7. https://doi.org/10.22159/ijap.2018v10i3.25024.

Beg, S., Almalki, W.H., Malik, A., Farhan, M., Aatif, M., Rahman, Z., Alruwaili, N.K., Alrobaian, M., Tarique, M., Rahman, M., 2020. 3D printing for drug delivery and biomedical applications. Drug Discovery Today 25 (9), 1668–1681. https://doi.org/10.1016/j.drudis.2020.07.007.

Builders, P.F., Arhewoh, M.I., 2016. Pharmaceutical applications of native starch in conventional drug delivery. Starch/Staerke 68 (9–10), 864–873. https://doi.org/10.1002/star.201500337.

Censi, Roberta, Gigliobianco, Maria Rosa, Casadidio, Cristina, Di Martino, Piera, 2018. Hot Melt Extrusion: Highlighting Physicochemical Factors to Be Investigated While Designing and Optimizing a Hot Melt Extrusion Process. Pharmaceutics 10, 89–116. https://doi.org/10.1002/star.201500337.

Chen, H., Xie, F., Chen, L., Zheng, B.o., 2019. Effect of rheological properties of potato, rice and corn starches on their hot-extrusion 3D printing behaviors. J. Food Eng. 244, 150–158.

Cheng, L., Wang, X., Gu, Z., Hong, Y., Li, Z., Li, C., Ban, X., 2022. Effects of different gelatinization degrees of starch in potato flour on the quality of steamed bread. Int. J. Biol. Macromol. 209 (PA), 144–152. https://doi.org/10.1016/j.ijbiomac.2022.03.208.

Cisneros, F.H., Zevillanos, R., Cisneros-Zevallos, L., 2009. Characterization of starch from two ecotypes of andean achira roots (Canna edulis). J. Agric. Food. Chem. 57 (16), 7363–7368. https://doi.org/10.1021/jf9004687.

Comoglu, T., Unal, B., 2015. Preparation and evaluation of an orally fast disintegrating tablet formulation containing a hydrophobic drug. Pharm. Dev. Technol. 20 (1), 60–64. https://doi.org/10.3109/10837450.2013.862636.

Cyriac, F., Lugt, P.M., Bosman, R., 2015. On a New Method to Determine the Yield Stress in Lubricating Grease. Tribol. Trans. 58 (6), 1021–1030. https://doi.org/10.1080/10402004.2015.1035414.

Dash, R., Foston, M., Ragauskas, A.J., 2013. Improving the mechanical and thermal properties of gelatin hydrogels cross-linked by cellulose nanowhiskers. Carbohydr. Polym. 91 (2), 638–645. https://doi.org/10.1016/j.carbpol.2012.08.080.

Dome, K., Podgorbunskikh, E., Bychkov, A., Lomovsky, O., 2020. Changes in the crystallinity degree of starch having different types of crystal structure after mechanical pretreatment. Polymers 12 (3), 1–12. https://doi.org/10.3390/polym12030641.

Domene-López, D., García-Quesada, J.C., Martin-Gullon, I., Montalbán, M.G., 2019. Influence of starch composition and molecular weight on physicochemical properties of biodegradable films. Polymers 11 (7), 1–17. https://doi.org/10.3390/polym11071084.

Elgaied-Lamouchi, D., Descamps, N., Lefevre, P., Rambur, I., Pierquin, J.-Y., Siepmann, F., Siepmann, J., Muschert, S., 2021. Starch-based controlled release matrix tablets: Impact of the type of starch. J. Drug Delivery Sci. Technol. 61, 102152. https://doi.org/10.1016/j.jddst.2020.102152.

Fina, F., Goyanes, A., Gaisford, S., Basit, A.W., 2017. Selective laser sintering (SLS) 3D printing of medicines. Int. J. Pharm. 529 (1–2), 285–293. https://doi.org/10.1016/j.ijpharm.2017.06.082.

Fuhrmann, K., Schulz, J.D., Gauthier, M.A., Leroux, J.C., 2012. PEG nanocages as non-sheddable stabilizers for drug nanocrystals. ACS Nano 6 (2), 1667–1676. https://doi.org/10.1021/nn2046554.

González, K., García-Astrain, C., Santamaria-Echart, A., Ugarte, L., Avérous, L., Eceiza, A., Gabilondo, N., 2018. Starch/graphene hydrogels via click chemistry with relevant electrical and antibacterial properties. Carbohydr. Polym. 202 (April), 372–381. https://doi.org/10.1016/j.carbpol.2018.09.007.

González, K., Guaresti, O., Palomares, T., Alonso-Varona, A., Eceiza, A., Gabilondo, N., 2020a. The role of cellulose nanocrystals in biocompatible starch-based clicked nanocomposite hydrogels. Int. J. Biol. Macromol. 143, 265–272. https://doi.org/10.1016/j.ijbiomac.2019.12.050.

González, K., Iturriaga, L., González, A., Eceiza, A., Gabilondo, N., 2020b. Improving mechanical and barrier properties of thermoplastic starch and polysaccharide nanocrystals nanocomposites. Eur. Polym. J. 123, 109415. https://doi.org/10.1016/j.eurpolymj.2019.109415.

Goyanes, A., Robles Martinez, P., Buanz, A., Basit, A.W., Gaisford, S., 2015. Effect of geometry on drug release from 3D printed tablets. Int. J. Pharm. 494 (2), 657–663. https://doi.org/10.1016/j.ijpharm.2015.04.069.

Hsu, M.N., Luo, R., Kwek, K.Z., Por, Y.C., Zhang, Y., Chen, C.H., 2015. Sustained release of hydrophobic drugs by the microfluidic assembly of multistage microgel/poly (lactic-co-glycolic acid) nanoparticle composites. Biomicrofluidics 9 (5), 1–7. https://doi.org/10.1063/1.4916230.

Ji, A., Zhang, S., Bhagia, S., Yoo, C.G., Ragauskas, A.J., 2020. 3D printing of biomass-derived composites: Application and characterization approaches. RSC Adv. 10 (37), 21698–21723. https://doi.org/10.1039/d0ra03620j.

Kalepu, S., Nekkanti, V., 2015. Insoluble drug delivery strategies: Review of recent advances and business prospects. Acta Pharmaceutica Sinica B 5 (5), 442–453. https://doi.org/10.1016/j.apsb.2015.07.003.

Karim, A.A., Toon, L.C., Lee, V.P.L., Ong, W.Y., Fazilah, A., Noda, T., 2007. Effects of phosphorus contents on the gelatinization and retrogradation of potato starch. J. Food Sci. 72 (2), C132–C138. https://doi.org/10.1111/j.1750-3841.2006.00251.x.

Kaur, N.S.J.S.L., Gill, N.S.S.B.S., 2003. Morphological, thermal and rheological properties of starches from different botanical sources. Food Chem. 81 (2), 219–231.

Khan, B., Bilal, M., Niazi, K., Samin, G., Jahan, Z., 2017. THERMOPLASTIC STARCH : A POSSIBLE BIODEGRADABLE FOOD PACKAGING MATERIAL — A REVIEW. https://doi.org/10.1111/jfpe.12447.

González, K., Retegi, A., González, A., Eceiza, A., Gabilondo, N., 2015. Starch and cellulose nanocrystals together into thermoplastic starch bionanocomposites. Carnohydrate POlymers 117, 83–90. https://doi.org/10.1016/j.carbpol.2014.09.055.

Larrañeta, E., Stewart, S., Ervine, M., Al-Kasasbeh, R., Donnelly, R., 2018. Hydrogels for hydrophobic drug delivery. Classification, synthesis and applications. *Journal of Functional.* Biomaterials 9 (1), 13. https://doi.org/10.3390/jfb9010013.

Larrea-Wachtendorff, D., Tabilo-Munizaga, G., Ferrari, G., 2019. Potato starch hydrogels produced by high hydrostatic pressure (HHP): A first approach. Polymers 11 (10), 1673. https://doi.org/10.3390/polym11101673.

Li, H., Fan, W., Zhu, X., 2020. Three-dimensional printing: The potential technology widely used in medical fields. J. Biomed. Mater. Res. - Part A 108 (11), 2217–2229. https://doi.org/10.1002/jbm.a.36979.

Li, H., Liu, S., Li, L., 2016. Rheological study on 3D printability of alginate hydrogel and effect of graphene oxide. Int. J. Bioprinting 2 (2), 54–66. https://doi.org/10.18063/IJB.2016.02.007.

Lima-Tenório, M.K., Tenório-Neto, E.T., Garcia, F.P., Nakamura, C.V., Guilherme, M.R., Muniz, E.C., Pineda, E.A.G., Rubira, A.F., 2015. Hydrogel nanocomposite based on starch and Co-doped zinc ferrite nanoparticles that shows magnetic field-responsive drug release changes. J. Mol. Liq. 210, 100–105. https://doi.org/10.1016/j.molliq.2014.11.027.

Liu, H., Xie, F., Yu, L., Chen, L., Li, L., 2009. Thermal processing of starch-based polymers. Progress in Polymer Science (Oxford) 34 (12), 1348–1368. https://doi.org/10.1016/j.progpolymsci.2009.07.001.

Liu, Z., Bhandari, B., Prakash, S., Mantihal, S., Zhang, M., 2019. Linking rheology and printability of a multicomponent gel system of carrageenan-xanthan-starch in extrusion based additive manufacturing. Food Hydrocolloids 87, 413–424.

Liu, Z., Zhang, M., Bhandari, B., Yang, C., 2018. Impact of rheological properties of mashed potatoes on 3D printing. J. Food Eng. 220, 76–82. https://doi.org/10.1016/j.jfoodeng.2017.04.017.

Lu, Z., Chen, W., Olivier, E., Hamman, J.H., 2008. Matrix polymeric excipients: Comparing a novel interpolyelectrolyte complex with hydroxypropylmethylcellulose. Drug Delivery 15 (2), 87–96. https://doi.org/10.1080/10717540801905009.

Mane, J.V., Chandra, S., Sharma, S., Ali, H., Chavan, V.M., Manjunath, B.S., Patel, R.J., 2017. Mechanical Property Evaluation of Polyurethane Foam under Quasi-static and Dynamic Strain Rates- An Experimental Study. Procedia Eng. 173, 726–731. https://doi.org/10.1016/j.proeng.2016.12.160.

Mazel, V., Guerard, S., Croquelois, B., Kopp, J.B., Girardot, J., Diarra, H., Busignies, V., Tchoreloff, P., 2016. Reevaluation of the diametral compression test for tablets using the flattened disc geometry. Int. J. Pharm. 513 (1–2), 669–677. https://doi.org/10.1016/j.ijpharm.2016.09.088.

O'Reilly, C.S., Elbadawi, M., Desai, N., Gaisford, S., Basit, A.W., Orlu, M., 2021. Machine learning and machine vision accelerate 3d printed orodispersible film development. Pharmaceutics 13 (12), 2187. https://doi.org/10.3390/pharmaceutics13122187.

Odeku, O.A., 2013. Potentials of tropical starches as pharmaceutical excipients: A review. Starch/Staerke 65 (1–2), 89–106. https://doi.org/10.1002/star.201200076.

Ogunsona, E., Ojogbo, E., Mekonnen, T., 2018. Advanced material applications of starch and its derivatives. Eur. Polym. J. 108 (August), 570–581. https://doi.org/10.1016/j.eurpolymj.2018.09.039.

Olmos-Juste, R., Alonso-Lerma, B., Pérez-Jiménez, R., Gabilondo, N., Eceiza, A., 2021. 3D printed alginate-cellulose nanofibers based patches for local curcumin administration. Carbohydr. Polym. 264, 118026. https://doi.org/10.1016/j.carbpol.2021.118026.

Onofre, F., Wang, Y.-J., 2009. Sustained Release Properties of Crosslinked and Substituted Starches. J. Appl. Polym. Sci. 117, 1558–1565.

Onofre, F., Wang, Y.J., Mauromoustakos, A., 2009. Effects of structure and modification on sustained release properties of starches. Carbohydr. Polym. 76 (4), 541–547. https://doi.org/10.1016/j.carbpol.2008.11.016.

Pandey, M., Choudhury, H., Fern, J.L.C., Kee, A.T.K., Kou, J., Jing, J.L.J., Her, H.C., Yong, H.S., Ming, H.C., Bhattamisra, S.K., Gorain, B., 2020. 3D printing for oral drug delivery: a new tool to customize drug delivery. Drug Delivery and Translational Research 10 (4), 986–1001. https://doi.org/10.1007/s13346-020-00737-0.

Parkash, V., Maan, S., Deepika, Yadav, S., Hemlata, H., Jogpal, V., 2011. Fast disintegrating tablets: Opportunity in drug delivery system. J. Adv. Pharm. Technol. Res. 2 (4), 223. https://doi.org/10.4103/2231-4040.90877.

Pérez, S., Bertoft, E., 2010. The molecular structures of starch components and their contribution to the architecture of starch granules: A comprehensive review. Starch/Staerke 62 (8), 389–420. https://doi.org/10.1002/star.201000013.

Raijada, D., Wac, K., Greisen, E., Rantanen, J., Genina, N., 2021. Integration of personalized drug delivery systems into digital health. Adv. Drug Deliv. Rev. 176, 113857. https://doi.org/10.1016/j.addr.2021.113857.

Raju, S., Reddy, P.S., Kumar, V.A., Deepthi, A., Reddy, K.S., Reddy, P.V.M., 2011. Flash release oral film of metoclopramide for pediatric use: Formulation and in- vitro evaluation. J. Chem. Pharm. Res 3 (4), 636–646.

Robles-Martinez, P., Xu, X., Trenfield, S.J., Awad, A., Goyanes, A., Telford, R., Basit, A.W., Gaisford, S., 2019. 3D printing of a multi-layered polypill containing six drugs using a novel stereolithographic method. Pharmaceutics 11 (6), 274. https://doi.org/10.3390/pharmaceutics11060274.

Salimi Jazi, M., Rezaei, A., Karami, G., Azarmi, F., Ziejewski, M., 2014. A computational study of influence of helmet padding materials on the human brain under ballistic impacts. Comput. Methods Biomech. Biomed. Eng. 17 (12), 1368–1382. https://doi.org/10.1080/10255842.2012.748755.

Schirmer, M., Höchstötter, A., Jekle, M., Arendt, E., Becker, T., 2013. Physicochemical and morphological characterization of different starches with variable amylose/

amylopectin ratio. Food Hydrocolloids 32 (1), 52–63. https://doi.org/10.1016/j.foodhyd.2012.11.032.

Seoane-Viaño, I., Gómez-Lado, N., Lázare-Iglesias, H., García-Otero, X., Antúnez-López, J.R., Ruibal, Á., Varela-Correa, J.J., Aguiar, P., Basit, A.W., Otero-Espinar, F. J., González-Barcia, M., Goyanes, A., Luzardo-álvarez, A., Fernández-Ferreiro, A., 2020. 3D printed tacrolimus rectal formulations ameliorate colitis in an experimental animal model of inflammatory bowel disease. Biomedicines 8 (12), 1–19. https://doi.org/10.3390/biomedicines8120563.

Seoane-Viaño, I., Januskaite, P., Alvarez-Lorenzo, C., Basit, A.W., Goyanes, A., 2021a. Semi-solid extrusion 3D printing in drug delivery and biomedicine: Personalised solutions for healthcare challenges. J. Control. Release 332 (February), 367–389. https://doi.org/10.1016/j.jconrel.2021.02.027.

Seoane-Viaño, I., Trenfield, S.J., Basit, A.W., Goyanes, A., 2021b. Translating 3D printed pharmaceuticals: From hype to real-world clinical applications. Adv. Drug Deliv. Rev. 174, 553–575. https://doi.org/10.1016/j.addr.2021.05.003.

Singh, N., Singh, J., Singh Sodhi, N., 2002. Morphological, thermal, rheological and noodle-making properties of potato and corn starch. J. Sci. Food Agric. 82 (12), 1376–1383. https://doi.org/10.1002/jsfa.1194.

Soares, G.A., De Castro, A.D., Cury, B.S.F., Evangelista, R.C., 2013. Blends of cross-linked high amylose starch/pectin loaded with diclofenac. Carbohydr. Polym. 91 (1), 135–142. https://doi.org/10.1016/j.carbpol.2012.08.014.

Szepes, A., Makai, Z., Blümer, C., Mäder, K., Kása, P., Szabó-Révész, P., 2008. Characterization and drug delivery behaviour of starch-based hydrogels prepared via isostatic ultrahigh pressure. Carbohydr. Polym. 72 (4), 571–578. https://doi.org/10.1016/j.carbpol.2007.09.028.

Taghizadeh, A., Favis, B.D., 2013. Effect of high molecular weight plasticizers on the gelatinization of starch under static and shear conditions. Carbohydr. Polym. 92 (2), 1799–1808. https://doi.org/10.1016/j.carbpol.2012.11.018.

Ugarte, L., Gómez-Fernández, S., Peña-Rodríuez, C., Prociak, A., Corcuera, M.A., Eceiza, A., 2015. Tailoring Mechanical Properties of Rigid Polyurethane Foams by Sorbitol and Corn Derived Biopolyol Mixtures. ACS Sustainable Chem. Eng. 3 (12), 3382–3387. https://doi.org/10.1021/acssuschemeng.5b01094.

Vadillo, J., Larraza, I., Calvo-Correas, T., Gabilondo, N., Derail, C., Eceiza, A., 2021. Role of in situ added cellulose nanocrystals as rheological modulator of novel waterborne polyurethane urea for 3D-printing technology. Cellulose 28 (8), 4729–4744. https://doi.org/10.1007/s10570-021-03826-6.

Van Renterghem, J., Vervaet, C., De Beer, T., 2017. Rheological Characterization of Molten Polymer-Drug Dispersions as a Predictive Tool for Pharmaceutical Hot-Melt Extrusion Processability. Pharm. Res. 34 (11), 2312–2321. https://doi.org/10.1007/s11095-017-2239-7.

Vithani, K., Goyanes, A., Jannin, V., Basit, A.W., Gaisford, S., Boyd, B.J., 2019. A Proof of Concept for 3D Printing of Solid Lipid-Based Formulations of Poorly Water-Soluble Drugs to Control Formulation Dispersion Kinetics. Pharm. Res. 36 (7) https://doi.org/10.1007/s11095-019-2639-y.

Wiranidchapong, C., Ruangpayungsak, N., Suwattanasuk, P., Shuwisitkul, D., Tanvichien, S., 2015. Plasticizing effect of ibuprofen induced an alteration of drug released from Kollidon SR matrices produced by direct compression. Drug Dev. Ind. Pharm. 41 (6), 1037–1046. https://doi.org/10.3109/03639045.2014.925917.

Yang, F., Zhang, M., Prakash, S., Liu, Y., 2018a. Physical properties of 3D printed baking dough as affected by different compositions. Innovative Food Sci. Emerg. Technol. 49 (January), 202–210. https://doi.org/10.1016/j.ifset.2018.01.001.

Yang, F., Zhang, M., Bhandari, B., Liu, Y., 2018b. Investigation on lemon juice gel as food material for 3D printing and optimization of printing parameters. LWT - Food Science and Technology 87, 67–76. https://doi.org/10.1016/j.lwt.2017.08.054.

Zheng, L., Yu, Y., Tong, Z., Zou, Q., Han, S., Jiang, H., 2019. The characteristics of starch gels molded by 3D printing. J. Food Process. Preserv. 43 (7), 1–11. https://doi.org/10.1111/jfpp.13993.

Zhu, X., Li, H., Huang, L., Zhang, M., Fan, W., Cui, L., 2020. 3D printing promotes the development of drugs. Biomed. Pharmacother. 131 (August), 110644 https://doi.org/10.1016/j.biopha.2020.110644.